

Automated on-chip rapid microscopy, phenotyping and sorting of *C. elegans*

Kwanghun Chung^{1,3}, Matthew M Crane^{2,3} & Hang Lu^{1,2}

Microscopy, phenotyping and visual screens are frequently applied to model organisms in combination with genetics. Although widely used, these techniques for multicellular organisms have mostly remained manual and low-throughput. Here we report the complete automation of sample handling, high-resolution microscopy, phenotyping and sorting of *Caenorhabditis elegans*. The engineered microfluidic system, coupled with customized software, has enabled high-throughput, high-resolution microscopy and sorting with no human intervention and may be combined with any microscopy setup. The microchip is capable of robust local temperature control, self-regulated sample-loading and automatic sample-positioning, while the integrated software performs imaging and classification of worms based on morphological and intensity features. We demonstrate the ability to perform sensitive and quantitative screens based on cellular and subcellular phenotypes with over 95% accuracy per round and a rate of several hundred worms per hour. Screening time can be reduced by orders of magnitude; moreover, screening is completely automated.

Forward genetics by screening mutagenized populations has long been a powerful technique. Additionally, reverse genetic approaches such as RNA interference have recently become prevalent in the study of small genetic model organisms such as *C. elegans*, especially in large-scale genomic studies of cell biology and development^{1–4}. Both types of methods require large sample sizes; however, high-resolution *in vivo* microscopy, phenotyping and screening are often low-throughput and are hence the current bottlenecks for large-scale genetic studies in multicellular model organisms. We anticipate even greater demand for high-throughput approaches as studies move from single genes and pathways to interactions and networks^{2,4–7}. The key challenge is twofold: there is a need not only for hardware that can robustly handle live worms in a way compatible with standard readouts (for example, high-resolution optical microscopy) to obtain high-content data in a high-throughput manner, but also for software that controls, automates and streamlines the manipulations, data acquisition, data storage, interpretation and quantitative analysis.

One existing commercial system that moves toward automation and high-throughput analysis is complex object parametric

analyzer and sorter, or COPAS (Union Biometrica), which is a fluorescence-activated cell sorter modified to handle small organisms. This system has been successfully used in large-scale studies of promoter activities and gene expression^{7–9}. Although powerful, COPAS is currently limited by its tissue-level, one-dimensional resolution capability and low data content per sample. When single-cell and subcellular imaging resolution is required, which is likely to be the case for studying cell fate in development or synapse structure and function^{4,10–16}, a new approach is required. In the last few years, a few microfluidic systems have been developed to study fly development¹⁷, zebrafish embryo development¹⁸ and behavior of worms^{19,20}, and to image worms^{21–25}. These systems have the general advantages of microfluidics (for example, laminar flow, proper length scale and possible integration of functions) and have grown increasingly sophisticated in their design as well as in the quality and speed of data analysis, to allow biologists to tackle complex problems.

Thus far, however, no microsystems (particularly automated ones) meet the specific requirements of large-scale visual screens. Previous work describes how microfluidic systems might be used for imaging *C. elegans* by implementing a parallel channel design²³ or for high-throughput screening using an intricate sequence of valve and flow maneuvers²⁴. Sorting, however, remains to be demonstrated. Additionally, the automation of sorting processes, a prerequisite for high-throughput methods, presents large challenges in the integration of functions, in robust and efficient sample preparation and handling, and in the speed of automatic decision-making, which ultimately governs the true throughput of such experiments.

We present here an integrated and automated microsystem for performing high-throughput microscopy at high resolution and for sorting based on phenotype (Fig. 1a,b). Our polydimethylsiloxane (PDMS) microfluidic chip (Fig. 1c,d) uses on-chip valves to control a suspension of nematodes and differs from previous work in the integration of several key design features that enable robust operation, which is critical for high-throughput experiments. Additionally, rather than using computer control solely as a mechanism to open and close valves²⁴, we developed a sophisticated control algorithm to automate the entire process of image acquisition, analysis and sorting, which allowed the system to

¹School of Chemical and Biomolecular Engineering, and ²Interdisciplinary Program in Bioengineering, Georgia Institute of Technology, 311 Ferst Dr. NW, Atlanta, Georgia 30332, USA, ³These authors contributed equally to this work. Correspondence should be addressed to H.L. (hang.lu@gatech.edu).

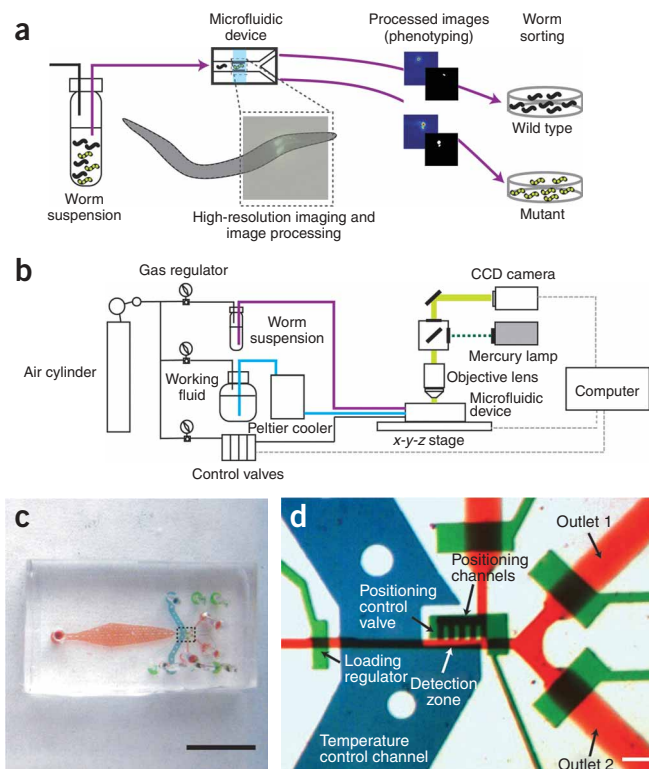


Figure 1 | Schematics of the system and the microchip. (a) A mixed population of worms is injected into the device, worms are imaged, phenotyped and then sorted. (b) System block diagram showing the on-chip and off-chip components. (c) Photograph of the microdevice. (d) Optical micrograph of the microchip's active region (boxed region in c). The channels were filled with dye to show specific features: blue, temperature control channel; green, valves; and red, sample-loading channel. Scale bars, 5 mm (c) and 100 μm (d).

the chip, so as to minimize the travel of the motorized stage to locate the worm and thereby reduce the processing time and increase throughput. This is achieved naturally by the position of the worm relative to the positioning channels: when no worm is loaded, the positioning channels have a larger pressure drop and therefore larger flow, dragging the worm toward the far end; when a worm is loaded, the pressure force equalizes, and the worm no longer experiences a substantial force (**Supplementary Fig. 2** online). Worms are loaded largely head-first, and the orientation is taken into consideration by the software for each application.

Third, the device has an integrated local temperature-control system whereby worms are cooled to $\sim 4^\circ\text{C}$ to immobilize them for imaging (**Supplementary Fig. 3** online). Immobilization is achieved without anesthetic drugs and thus minimizes potential adverse developmental effects of these drugs. Although mechanical immobilization of the worms by applying suction reduced movement, it proved inadequate for high-magnification imaging with simple epifluorescence microscopy (**Supplementary Video 1** online). The use of brief cooling, however, proved effective at stopping motion (**Supplementary Video 2** online) and we observed no discernible differences in the fluorescence pattern of cooled worms compared to those immobilized with sodium azide (**Supplementary Fig. 4** online). Fourth, the microchip and the setup are compatible with any standard microscopy setup with no modification necessary, including simple compound epifluorescence microscopy as well as more expensive multiphoton or confocal microscopy. Fifth, the microchip has no permanent small features ($< 20\ \mu\text{m}$) and therefore is easy to fabricate, less likely to be clogged by debris and can operate very robustly (**Supplementary Videos 3** and **4** online). Last, losses of worms through our system were minimal ($\sim 3\%$) and the viability of all of the sorted worms was $\sim 100\%$.

To allow the microsystem to operate free from the need for any human intervention, we developed a software system comprising control, acquisition and processing modules. The image-processing module consists of several subroutines, which can be modified to detect phenotypes based on various reporters and expression profiles. In addition to sorting and classifying worms based on intensity or location of a reporter, it is possible to look at features describing cell or synapse morphology.

Rapid, large-scale expression pattern analysis

Gene expression pattern analysis is a common technique in genetic and genomic studies^{2,4,5}. Typically one would be interested in the intensity, location and timing of appearance of a (fluorescent) reporter. We tested the capacity of our system to rapidly analyze the gene expression patterns in a population of worms carrying a reporter transgene *kyls342* (ref. 26). In this strain GFP is expressed in sensory neurons AQR, URXL/R and PQR¹⁹, and in coelomocytes (coinjection marker *punc-122-gfp*). In addition, we observed background fluorescence in the intestine (**Fig. 3a**).

operate without human intervention. We implemented classification and sorting of worms based on many characteristics, such as intensity and patterns of fluorescent markers. We show here three realistic examples of how our automated system can be used in genetic analysis and screens of *C. elegans*. This microfluidics-enabled computer-automated approach can perform screens based on cellular and subcellular phenotypes with over 95% accuracy per round and a rate of several hundred worms per hour, and thus provides a means for high-throughput studies.

RESULTS

System design for rapid and high-resolution microscopy

In each experiment, worms are manipulated by a simple scheme of load, image, phenotype and release or sort (**Fig. 2**): first, a single worm is automatically loaded into the engineered microchip by a constant pressure-driven flow; then the worm is briefly (and reversibly) immobilized while multidimensional images of the worms are acquired on-chip; then phenotyping and sorting take place, and images are stored for analysis. This cycle repeats automatically.

The robustness and automation of our system relies greatly on integrated closed-loop control software as well as engineered hardware design of the microchip. The chip has 6 salient features that ensure a consistent and reliable operation for an extended period of time. First, it automatically self-regulates the loading of nematodes by a simple passive loading-regulator design (**Supplementary Fig. 1** online), as compared to using the complex multistep loading mechanism that requires additional image acquisition, analysis and valve actuation²⁴. Constant pressure drives the flow so that no intervention is necessary for the microchip to allow one and only one worm to occupy the imaging area at a time. Second, the setup automatically positions the nematodes in an identical position in

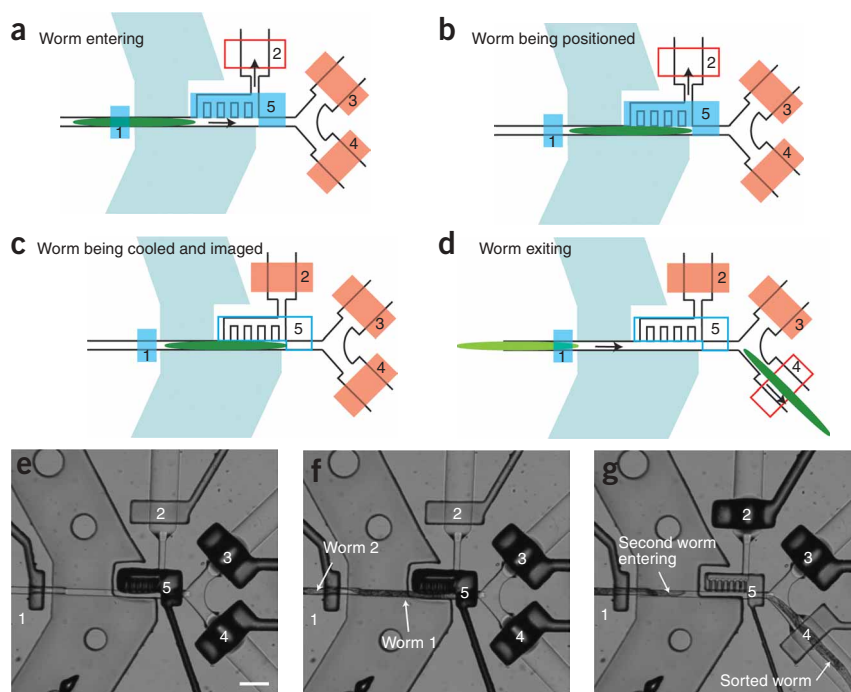


Figure 2 | Microdevice operation. (a–d) Schematic diagrams summarizing the valve control sequence in the worm-sorting process (dark blue, partially closable and tunable valves; red, fully closable valves; open boxes, valves in closed position; colored boxes, valves in open position). Valve 1 is always partially closed to prevent multiple worms from entering. Valve 2 on the positioning channel is opened to generate a pressure gradient to guide a worm into the observation chamber (a,b). Once the worm is positioned in the observation chamber, all the valves for fluid to exit the observation chamber are closed to eliminate flow fluctuation (c). One of the exit valves (3 or 4) is opened to allow the imaged worm to leave (d). Once the worm leaves the observation chamber the valves return to the worm entering state. (e–g) Frames from videos showing the chamber while waiting for a worm to enter (e), with a loaded worm preventing a second worm from entering (f), and a second worm automatically moving into the detection zone after the previous worm exited the detection zone (g). Scale bar, 100 μm .

In this experiment, worms were freely moving and we used no immobilization; we acquired all images at room temperature (20–22 °C) and 10 \times magnification. The software processed images (see **Supplementary Methods** online) to distinguish specific neurons not only from background autofluorescence and from coelomocytes but also from each other. We could identify the neurons in each image (**Fig. 3b–m**). We found that GFP expression in the URX neurons was consistent, but expression in AQR and PQR neurons was stochastic, with four possible combinations: GFP expression in neither, both or one of the two cells (**Fig. 3b–e,n**).

We sorted the worms based on classification of the PQR expression pattern. We collected two populations: one identified by the software as having GFP expression in PQR (on) and one identified as without GFP expression in this cell (off) (**Table 1**). The worms were sorted at a speed of ~ 900 worms/h; both the loading and the image acquisition were rapid and entirely automated. Over 90% of worms were loaded into the observation chamber within 1 s after the previous worm exited (**Fig. 3o**; $n = \sim 8,200$). The false positive and false negative rates of sorting were low (**Table 1**). In addition, because the worms remained at room temperature with no exposure to anesthetics, there was no concern about the alteration of the expression pattern, and it was possible to collect and reimagine the worms at a later time. This mode of operation of our system can be adapted for several types of studies using transgene

reporters, for instance, the analysis of promoter activities and of genetic interactions⁷.

Phenotyping and sorting based on reporter expression

Whole-genome coverage in forward or reverse genetic screens usually requires examining large numbers of worms to find the rare few with dissimilar phenotypes. To demonstrate the microsystem's ability to perform an automated rare sort, we performed a mock screen by sorting a small number of mutant worms mixed in a background of worms of wild-type genotype. *C. elegans* has many bilaterally symmetric cells, which exhibit functional asymmetry, such as the AWC neurons. We used worms expressing the *str-2-GFP* reporter in the AWC neurons. In wild-type worms, one of the two neurons expresses *str-2* (AWC-on), whereas mutations in the *slo-1* gene produce the 2-AWC-on phenotype¹⁰, where both AWC cells express *str-2*. In our experiment, the microsystem sorted a small fraction ($\sim 1.5\%$) of *slo-1*^{-/-} 2-AWC-on worms from wild-type 1-AWC-on-1-AWC-off worms. This experiment also demonstrates the ability to screen using high-resolution imaging based on signals from different cells at similar in-plane locations but different depth and carried out on a common epifluorescence compound microscope.

Because the two AWC neurons are located at the same position along the anterior-posterior axis and are $< 20 \mu\text{m}$ apart, low-magnification microscopy cannot be used to distinguish the 1-on from the 2-on phenotype. We therefore used a 100 \times oil objective (numerical aperture, NA = 1.4) and designed the microchip to be compatible with high-resolution microscopy. Additionally, complete immobilization of worms is necessary because any movement would cause blurring of the images and make identification of the neurons impossible. We immobilized the worms by transiently cooling them on-chip to ~ 4 °C. Once the worm was immobilized, sparse z-stack images along the body of each worm were obtained to determine the location of the head (**Fig. 4a**). The stage then centered on what were identified as AWC neurons within the field of view, and a denser z-stack of images was acquired (**Fig. 4b**). Because of the chip design, very little if any optical distortion occurred. To determine whether the worm had the 2-AWC-on (*slo-1*^{-/-}; **Fig. 4c,d**) or the 1-on-1-off (wild-type) phenotype, images were analyzed by flattening and thresholding. The worms were then sorted according to their phenotypes. The z-stack images of all worms were saved to a hard drive during phenotyping and sorting to allow the user to retrieve them later for additional analysis or manual verification. Representative z-stack images acquired during the experiments are available in **Supplementary Videos 5** and **6** online. During this experiment, most time was consumed by scanning the entire worm and saving images to disk; the

Table 1 | Number of worms in input and outputs in high-throughput automated sorting experiments

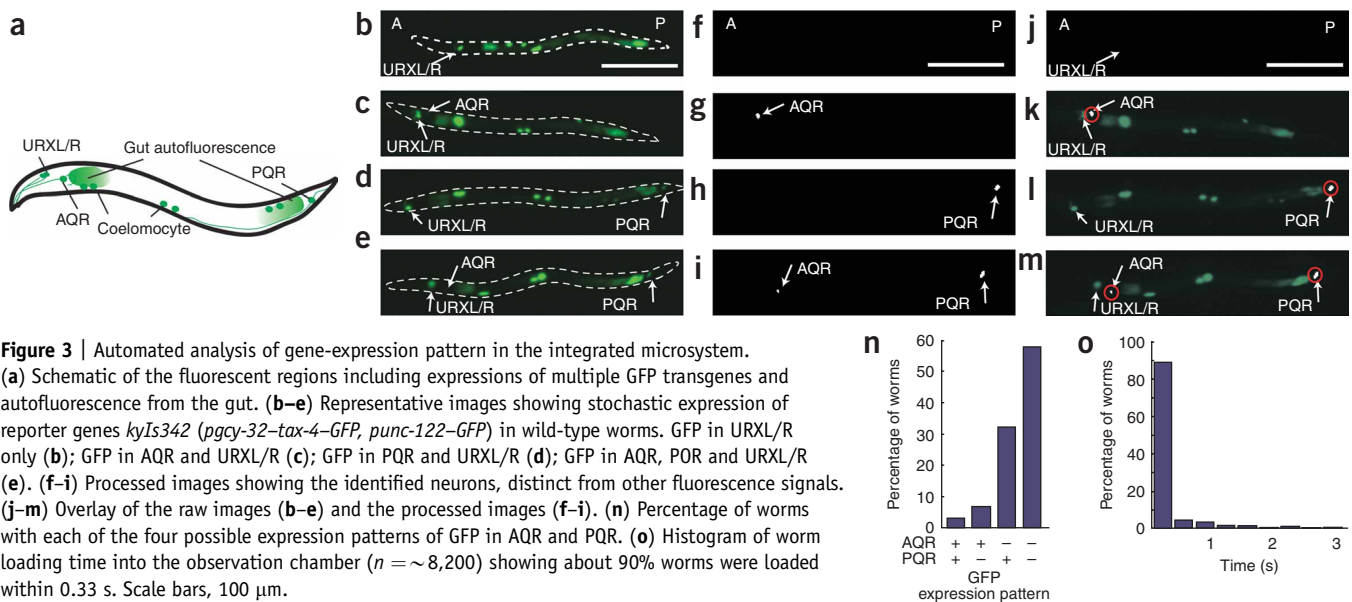
Trial	Total number input	Sort output 1		Sort output 2		Total number sorted	Percent in mix	False positives (%)	False negatives (%)	Enrichment (%)		
		GFP ⁺ as GFP ⁺	GFP ⁻ as GFP ⁺	GFP ⁻ as GFP ⁻	GFP ⁺ as GFP ⁻							
PQR GFP ⁺	1	~2,500	640	86	1,601	119	2,446	31.0	11.8	6.9	284	
versus	2	~2,100	629	62	1,314	79	2,084	34.0	9.0	5.7	268	
PQR GFP ^{-a}	3	~2,500	794	61	1,541	104	2,500	35.9	7.1	6.3	259	
	4	~1,800	508	39	1,176	73	1,796	32.3	7.1	5.8	287	
Average									8.8 ± 2.2	6.2 ± 0.6	274 ± 14	
			Percent mutant	2-AWC-on as 2-AWC-on	1-AWC-on as 2-AWC-on	1-AWC-on as 1-AWC-on	2-AWC-on as 2-AWC-on					
1-AWC-on	1	~1,200	~1.5	19	90	1,021	2	1,132	1.9	82.6	0.2	940
versus	2	~1,400	~1.5	16	110	1,277	1	1,404	1.2	87.3	0.1	1,049
2-AWC-on ^b	3	~1,200	~1.5	14	77	1,091	1	1,183	1.3	84.6	0.1	1,213
Average										84.8 ± 2.4	0.1 ± 0.1	1,070 ± 140
			Percent mutant	<i>unc-16</i> ^{-/-} as <i>unc-16</i> ^{-/-}	Wild type as <i>unc-16</i> ^{-/-}	Wild type as wild type	<i>unc-16</i> ^{-/-} as wild type					
Wild type	1	~1,400	~30	410	2	930	29	1,371	32.0	0.5	3.0	311
versus	2	~1,400	~25	308	32	971	21	1,332	24.7	9.4	2.1	367
<i>unc-16</i> ^{-/-c}	3	~1,400	~25	309	37	1,030	24	1,400	23.8	10.7	2.3	375
Average										6.9 ± 5.6	2.5 ± 0.5	350 ± 35

^aSee Figure 3. ^bWild type (1-AWC-on) versus *slo-1*^{-/-} (2-AWC-on) sorting based on number of AWC-on neurons (see Fig. 4). ^cWild type versus *unc-16*^{-/-} sorting based on synaptic features (see Fig. 5). The false positive and false negative percentages were determined from the number of missorted worms divided by the total number of worms sorted as positive and negative.

throughput could be increased by optimizing the procedure to locate the neurons and by reducing the number of images saved for each worm.

Based on the GFP expression patterns, we sorted a mixture of ~1.5% 2-on *slo-1*^{-/-} mutant and 98.5% wild-type (1-on) age-synchronized adult worms (Table 1). With online processing and decision-making without human supervision, we found that, even with multiple z-stack image acquisition and intense

computation required, the system achieved a sorting speed of ~150 worms/h. We verified sorting accuracy by examining the collected worms for the roller phenotype as the *slo-1*^{-/-} strain used in this experiment also carries this unrelated phenotype. In all trials ($n > 1,000$ worms each), the false negative rate (2-AWC-on worms being sorted as 1-AWC-on-1-AWC-off worms) was <0.2%, indicating that the system captured almost all the mutants. The mutant ratio in the final sorted population was



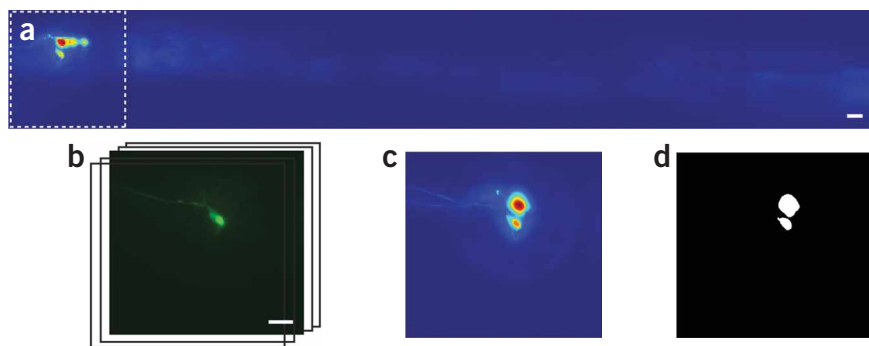


Figure 4 | Automated three-dimensional imaging and sorting with cellular resolution in the integrated microsystem: image processing and decision-making to sort worms based on the number of AWC neurons expressing *pstr-2-gfp*. (a) Images of a *slo-1^{-/-}* mutant with two AWC-on neurons. Flattened series of sparse z-stack images along the body of worms showing the cell bodies and the neurites. Red represents high contrast, and blue represents low contrast. (b) Denser z-stack images near the head of the worms so that it is possible to establish the number of AWC-on neurons. Only one frame from the z stack is shown. (c) Flattened dense z-stack images near the head (same as dashed region in a). (d) Thresholded image showing identified neurons. Scale bars, 10 μm .

greatly enriched (Table 1). If desired, accuracy of the sorting can be improved by altering sorting criteria and implementing multiple rounds of sorting.

Phenotyping and sorting based on synaptic features

Genetic screens are becoming more difficult to perform because the phenotypes of interest are becoming subtler. For example, many of

(H. Brown and Y. Jin, personal communication), which is a major feature we used for sorting. Age-synchronized mixed populations were sorted according to their synaptic marker phenotypes at a rate of ~ 400 worms/h. Cooling the chamber immobilized the worms, which enabled subcellular resolution (Fig. 5i,j). Representative z-stack images acquired in the device during the experiments are available in Supplementary Videos 7 and 8 online. We used online

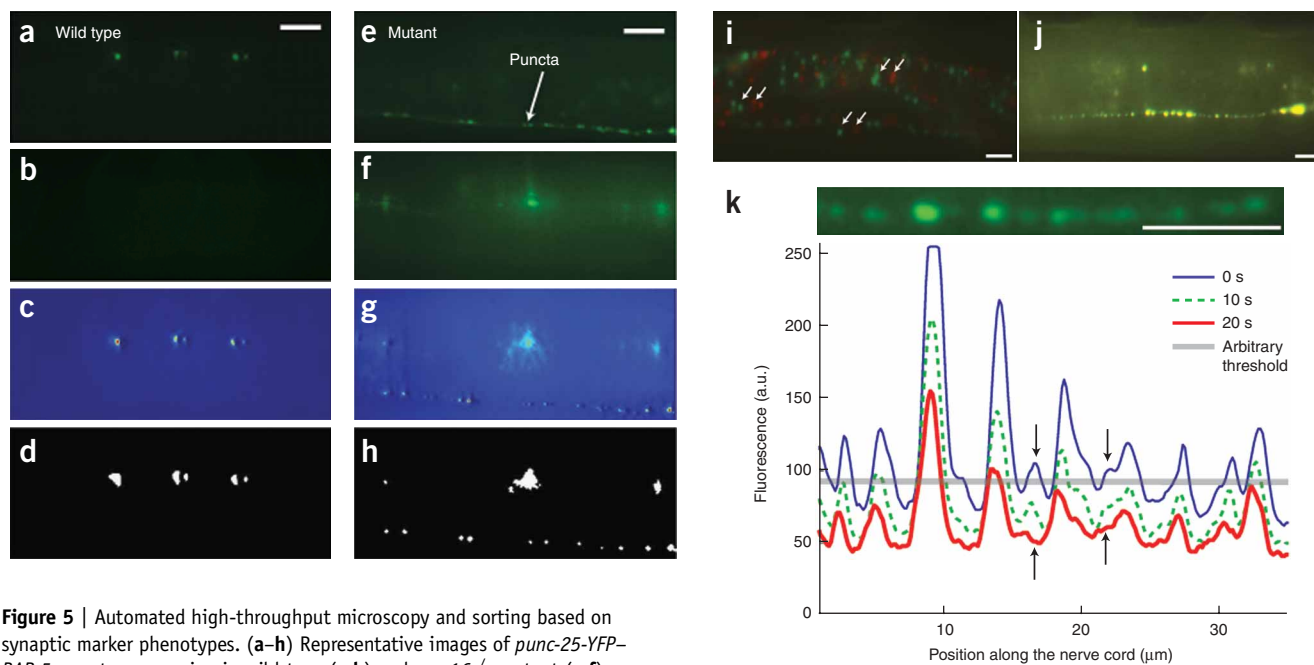


Figure 5 | Automated high-throughput microscopy and sorting based on synaptic marker phenotypes. (a–h) Representative images of *punc-25-YFP-RAB-5* reporter expression in wild-type (a,b) and *unc-16^{-/-}* mutant (e,f) worms at two focal planes 20 μm apart. Processed images from the corresponding worms to find cell bodies and puncta along the nerve cord (c,d,g,h). Wild-type worms show fluorescence in cell bodies (a–d), and mutant worms have increased marker intensity in the nerve cord, showing puncta structures along its length (e–h), which were the basis for sorting. (i) Two frames taken of a worm mechanically clamped with no cooling. The first frame was colored red and the second frame 270 ms later was colored green. Arrows point to features moved during the 270 ms. (j) Two frames 10 s apart (also colored red and green) of a worm imaged with cooling to 4 $^{\circ}\text{C}$, showing no discernible movement. (k) Puncta structures of the nerve cord in a mutant worm before photobleaching (top). Quantification of puncta fluorescence from line scans as photobleaching occurred (bottom). The use of a threshold to determine the number of puncta structures could result in puncta being miscounted depending on the extent of photobleaching. Arrows point to two small punctal structures that would not be identified after deliberate photobleaching for 20 s. Scale bars, 10 μm .

the synaptic or other subcellular reporters exhibit features that are sub-micrometer-sized, and reporters for these features are dim and easily photobleached. Thus, not only is manual phenotyping often too slow, but it is also often not precise or objective enough to detect quantitative changes. Using our automated system, we eliminated the need to seek the targeted region in the sample, thereby greatly reducing exposure time and the extent of photobleaching.

To test the ability to screen based on subcellular changes, we sorted strains carrying an integrated reporter transgene *juls198 (punc-25-YFP-rab-5)*, which is expressed in the GABAergic motoneurons and labels a subset of synaptic endosomes²⁷. In the wild-type background, YFP-RAB-5 was faint in the nerve cord (Fig. 5a–d), but *unc-16^{-/-}* mutants had increased marker intensity along the nerve cord (Fig. 5e–h)

image processing (Fig. 5c,d,g,h) to identify the puncta along the nerve cord. To verify the sorting accuracy, we manually analyzed the sorted worms by the recorded images and by examining uncoordinated behavior. Table 1 shows sorting results for each of the three trials; the overall sorting accuracy (total correctly sorted over total worms sorted) was 96.5% for a single round.

Reporter intensity can be quantitatively analyzed in the images that are recorded (Fig. 5k). The number of puncta and size distribution of the puncta were automatically analyzed. By implementing additional classification features (such as average intensity, distance between features, number of features and ellipticity of features), it will be possible to sort different *C. elegans* mutants from wild-type worms. Although we based the decision boundaries on known distributions between wild-type and mutant classes based on a set of training data (Supplementary Fig. 5 online), modeling the distribution of a wild-type class based on these features will allow us to screen for new types of mutants.

Analysis of reporter intensity often can be strongly influenced by photobleaching of markers and inconsistent handling between samples^{4,28}. For instance, we deliberately photobleached strain CZ5264 (Fig. 5k). Our system minimizes photobleaching by avoiding manual focusing; data with minimal bleaching (for example, 30 ms as in this experiment) can be recorded and used for subsequent analysis. All worms receive the same handling in the automated microsystem and images are analyzed uniformly using the same criteria, thus reducing noise and biases that may be introduced by manual operation.

DISCUSSION

Our system is microscope- and camera-independent; it is compatible with all typical microscopy setups in biology laboratories, such as confocal or two-photon microscopy, simple epifluorescence microscopy or even stereo microscopy. Because the add-ons to already existing microscopy tools only include the microchip, some simple commercially available parts and widely used software such as Matlab (Mathworks, Inc.), the system is very inexpensive to replicate. In addition, tailored complex image-analysis routines for specific screens can be integrated because the control algorithm is modular. To adapt the system for *C. elegans* of different sizes as well as for other small organisms (for example, *Drosophila melanogaster* and *Danio rerio* embryos), one would need to simply change the geometry (for example, height and length) of certain parts of the chip, while using the same basic features and functions. Similarly, retuning the software modules (such as intensity and size thresholds) should be straightforward. This customizability provides our system with a wide range of applications.

Compared to manual phenotyping and screening experiments that typically require many months to complete, our system without further optimization can already perform such experiments without human intervention in a few days to a few weeks, depending on the complexity and subtlety of the phenotypes. Photobleaching of fluorescent markers and other artifacts owing to a researcher's handling are minimized by avoiding 'feature-seeking' steps. More importantly, this microsystem and the automation should allow for rapid complex genetic screens based on subtle phenotypes that would be otherwise difficult or impossible to detect. For example, human eyes are imprecise at detecting absolute changes in brightness; by using our system, one can potentially screen for mutants that have altered intensity of

reporters or that have slightly altered morphology. In gene expression analysis, use of this system can also drastically improve the quality of expression-pattern data because of the less subjective nature of our approach. Compared to the only commercially available automated sorting system, COPAS, our system has much higher optical resolution and therefore an expanded repertoire of applications. Additionally, owing to the modular nature of our system, supplementary devices could be incorporated in series with it to fulfill additional needs, such as administering small-molecule libraries to distinct populations before screening for pharmacological studies. In addition, it could be coupled with laser ablations and behavioral studies. Our method could eliminate a substantial bottleneck in genetic analyses and enable large-scale quantitative experiments in developmental biology, functional genomics and related fields.

METHODS

***C. elegans* strains, culture and sample preparation.** We grew the worms according to standard protocols at 15, 20 or 25 °C²⁹. We used the following strains in this work: CX6858 *tax-4(ks28); kyls342(pgcy-32-tax-4-GFP, punc-122-GFP)*, CX3695 *kyls140(str-2-GFP + lin-15(+))*, CX3940 *kyls140; rol-6(e187); slo-1(ky399)*, CZ5261 *juIs198(punc-25-YFP-rab-5)* and CZ5264 *unc-16(ju146); juIs198*. We suspended age-synchronized L4 worms in M9 solution containing 0.5% (wt/wt) BSA for each experiment. We used an in-line filtering device to filter out dust (Supplementary Fig. 6 online).

Fabrication of devices. We fabricated the microfluidic device using modified multilayer soft lithography³⁰. Briefly, we fabricated two different molds by conventional photolithographic processes to create the worm-loading layer and the control layer. We partially cured the control layer (5 mm; Sylgard 184 A and B, 5:1; Dow Corning) and then bonded it to the 20- μ m-thick PDMS membrane (20:1). We spin-cast the sample-loading layer PDMS (20:1) as a 60- μ m-thick layer, fully cured it, peeled it off, turned it upside down and bonded it to the control layer using oxygen plasma treatment. We punched holes for access to the loading and control channels. Then we bonded the assembled layers onto a cover glass to form the device.

System control, image acquisition and analysis. We interfaced all off-chip and on-chip components to a personal computer and controlled all components by custom-designed Matlab routines (available upon request). The Matlab code for worm sorting contained three basic elements: waiting for worm's entrance to detection zone, image acquisition and image processing and allowing the worm to exit before returning to the initial state. We tailored the image analysis for phenotyping or quantitative gene expression analysis for each application. We manually verified sorted worms (Supplementary Fig. 7 online).

Additional methods. Descriptions of the software and system specifications are available in **Supplementary Methods**.

Note: Supplementary information is available on the Nature Methods website.

ACKNOWLEDGMENTS

We acknowledge US National Science Foundation (DBI-0649833) and National Institutes of Health (NS058465) for funding, Caenorhabditis Genetics Center, Y. Jin (University of California San Diego), and C.I. Bargmann (Rockefeller University) for

providing strains, H. Brown and Y. Jin for sharing unpublished observations, J. Stirman for technical assistance, and V. Breedveld, R. Butera, T. Streelman and Y. Thio for commenting on the manuscript. M.M.C. is a National Science Foundation graduate fellow.

AUTHOR CONTRIBUTIONS

K.C., M.M.C. and H.L. designed the experiments. K.C. fabricated the devices, M.M.C. implemented the software, and K.C. and M.M.C. conducted the experiments. K.C., M.M.C. and H.L. analyzed the data and wrote the paper.

Published online at <http://www.nature.com/naturemethods/>
Reprints and permissions information is available online at
<http://npg.nature.com/reprintsandpermissions/>

1. Fire, A. *et al.* Potent and specific genetic interference by double-stranded RNA in *Caenorhabditis elegans*. *Nature* **391**, 806–811 (1998).
2. Sonnichsen, B. *et al.* Full-genome RNAi profiling of early embryogenesis in *Caenorhabditis elegans*. *Nature* **434**, 462–469 (2005).
3. Kamath, R.S. & Ahringer, J. Genome-wide RNAi screening in *Caenorhabditis elegans*. *Methods* **30**, 313–321 (2003).
4. Sieburth, D. *et al.* Systematic analysis of genes required for synapse structure and function. *Nature* **436**, 510–517 (2005).
5. Hunt-Newbury, R. *et al.* High-throughput *in vivo* analysis of gene expression in *Caenorhabditis elegans*. *PLoS Biol.* **5**, e237 (2007).
6. Piano, F., Gunsalus, K.C., Hill, D.E. & Vidal, M. *C. elegans* network biology: a beginning. in *WormBook* (ed. The *C. elegans* Research Community). Published online 21 August, 2006 (doi:10.1895/wormbook.1.118.1).
7. Dupuy, D. *et al.* Genome-scale analysis of *in vivo* spatiotemporal promoter activity in *Caenorhabditis elegans*. *Nat. Biotechnol.* **25**, 663–668 (2007).
8. Mango, S.E. A green light to expression in time and space. *Nat. Biotechnol.* **25**, 645–646 (2007).
9. Duverger, Y. *et al.* A semi-automated high-throughput approach to the generation of transposon insertion mutants in the nematode *Caenorhabditis elegans*. *Nucleic Acids Res.* **35**, e11 (2007).
10. Troemel, E.R., Sagasti, A. & Bargmann, C.I. Lateral signaling mediated by axon contact and calcium entry regulates asymmetric odorant receptor expression in *C. elegans*. *Cell* **99**, 387–398 (1999).
11. Klassen, M.P. & Shen, K. Wnt signaling positions neuromuscular connectivity by inhibiting synapse formation in *C. elegans*. *Cell* **130**, 704–716 (2007).
12. Zhao, H. & Nonet, M.L. A retrograde signal is involved in activity-dependent remodeling at a *C. elegans* neuromuscular junction. *Development* **127**, 1253–1266 (2000).
13. Zhen, M. & Jin, Y. The liprin protein SYD-2 regulates the differentiation of presynaptic termini in *C. elegans*. *Nature* **401**, 371–375 (1999).
14. Schaefer, A.M., Hadwiger, G.D. & Nonet, M.L. *rpm-1*, a conserved neuronal gene that regulates targeting and synaptogenesis in *C. elegans*. *Neuron* **26**, 345–356 (2000).
15. Shen, K. & Bargmann, C.I. The immunoglobulin superfamily protein SYG-1 determines the location of specific synapses in *C. elegans*. *Cell* **112**, 619–630 (2003).
16. Hobert, O., Johnston, R.J. & Chang, S. Left-right asymmetry in the nervous system: The *Caenorhabditis elegans* model. *Nat. Rev. Neurosci.* **3**, 629–640 (2002).
17. Lucchetta, E.M., Lee, J.H., Fu, L.A., Patel, N.H. & Ismagilov, R.F. Dynamics of *Drosophila* embryonic patterning network perturbed in space and time using microfluidics. *Nature* **434**, 1134–1138 (2005).
18. Funfak, A., Brösing, A., Brand, M. & Köhler, J.M. Micro fluid segment technique for screening and development studies on *Danio rerio* embryos. *Lab Chip* **7**, 1132–1138 (2007).
19. Gray, J.M. *et al.* Oxygen sensation and social feeding mediated by a C-elegans guanylate cyclase homologue. *Nature* **430**, 317–322 (2004).
20. Zhang, Y., Lu, H. & Bargmann, C.I. Pathogenic bacteria induce aversive olfactory learning in *Caenorhabditis elegans*. *Nature* **438**, 179–184 (2005).
21. Chronis, N., Zimmer, M. & Bargmann, C.I. Microfluidics for *in vivo* imaging of neuronal and behavioral activity in *Caenorhabditis elegans*. *Nat. Methods* **4**, 727–731 (2007).
22. Heng, X. *et al.* Optofluidic microscopy—a method for implementing a high resolution optical microscope on a chip. *Lab Chip* **6**, 1274–1276 (2006).
23. Hulme, S.E., Shevkopyas, S.S., Apfeld, J., Fontana, W. & Whitesides, G.M. A microfabricated array of clamps for immobilizing and imaging *C. elegans*. *Lab Chip* **7**, 1515–1523 (2007).
24. Rohde, C.B., Zeng, F., Gonzalez-Rubio, R., Angel, M. & Yanik, M.F. Microfluidic system for on-chip high-throughput whole-worm sorting and screening at subcellular resolution. *Proc. Natl. Acad. Sci. USA* **104**, 13891–13895 (2007).
25. Guo, S.X. *et al.* Femtosecond laser nanoaxotomy lab-on-a-chip for *in vivo* nerve regeneration studies. *Nat. Methods* **5**, 531–533 (2008).
26. Chang, A.J., Chronis, N., Karow, D.S., Marletta, M.A. & Bargmann, C.I. A distributed chemosensory circuit for oxygen preference in *C. elegans*. *PLoS Biol.* **4**, e274 (2006).
27. Grill, B. *et al.* *C. elegans* RPM-1 regulates axon termination and synaptogenesis through the Rab GEF GLO-4 and the Rab GTPase GLO-1. *Neuron* **55**, 587–601 (2007).
28. Dittman, J.S. & Kaplan, J.M. Factors regulating the abundance and localization of synaptobrevin in the plasma membrane. *Proc. Natl. Acad. Sci. USA* **103**, 11399–11404 (2006).
29. Brenner, S. The genetics of *Caenorhabditis elegans*. *Genetics* **77**, 71–94 (1974).
30. Unger, M.A., Chou, H.P., Thorsen, T., Scherer, A. & Quake, S.R. Monolithic microfabricated valves and pumps by multilayer soft lithography. *Science* **288**, 113–116 (2000).